Design and Fabrication of a Novel Resonant Surface Sensitive to Out-of-plane Forces for the Indentation and Injection of Living Cells

Denis Desmaële, Mehdi Boukallel and Stéphane Régnier

Abstract— **We present a novel force sensor for cell indentation and cell injection. This force sensor is a monolithic structure that integrates two resonators. It provides a surface sensitive to out-of-plane forces where a living cell can be conveniently placed for manipulation. Normal forces applied upon the cell under study are estimated via frequency shifts of the resonators. In this paper, we develop a theoretical study for predicting and optimizing the structure's sensitivity. As a proof of concept, we also report the fabrication and experimental characterization of a first prototype. In ambient conditions, our prototype presently offers a quality factor of ∼700, and a linear sensitivity of ∼5.75 Hz $/ \mu$m. In addition, we report the implementation of a compact and low-cost optical fiber setup to monitor the resonators' frequency. Potential applications are illustrated with the measurement of forces applied on lobster eggs.**

I. INTRODUCTION

The injection of living cells can be considered as one of the most common biomanipulation tasks [1]. Indeed, the possibility to safely inject small volumes of foreign compounds into individual cells plays a prominent role in many life sciences such as genetics, transgenics, molecular biology or drug discovery.

During the penetration of the cellular membrane, the estimation of the interaction force between the cell and the injection micropipette is an essential information. Indeed, cells are prone to irremediable damages if excessive forces are applied during the injection process. Hence, to ensure higher success and survival rates, cell injection systems must be equipped with force measurement systems in order to implement force control.

To date, most cell injection systems have been designed to inject spherical suspended cells (e.g., embryos, oocytes). To estimate the force applied upon such cells, vision-based techniques that track cell deformations can be used. However, to recover the force solely from visual feedback, the elastic properties of the cell to be injected must usually be known *a priori* [2]. Moreover, the resolution of vision-based techniques is inherently limited by the optical components of the microscope. Therefore, the use of an additional *contact-based* force sensor is usually preferred.

Conventionally, for measuring the penetration force of embryos or oocytes, an injection micropipette is bonded to the free end of a compliant cantilever covered with sensitive films (e.g., [1], [3], [4]). The pressure tube which is connected to the micropipette for the delivery of liquid samples can however affect the penetration force measurement [5]. In addition, the sensitive cantilever bends during the penetration phase. Compared to a rigid glass micropipette, this bending can cause more puncture damages to the cell [5].

Other types of force sensors circumvent the drawbacks inherent to cantilevered micropipettes. For instance, the capacitive sensor reported in [6] allowed the authors to accurately measure puncture forces of embryos and oocytes. Nevertheless, the device was not designed to ensure the delivery of foreign materials into cells. This limitation appears to have been overcome in [7], but only for suspended cells. To the best of the authors' knowledge, the force-controlled injection of adherent cells with irregular morphology (e.g., mammalian cells such a fibroblasts, HeLa cells, endothelial cells) has only been recently reported in [8]. Nonetheless, the force sensitive setup is based on an expensive atomic force microscope.

We therefore find that the capability to measure cell penetration forces for different types of cells while ensuring the delivery of fluid samples in a cost-effective manner remains challenging. In this paper, we propose a novel type of force sensor designed to bring new solutions to this problem. Ultimately, this force sensor might offer the following advantages:

- Both adherent and suspended cells could be targeted.
- Low-cost and commercially available glass micropipettes could be conveniently used while avoiding problems discussed in [5].

The remainder of the paper is organized as follows. First, a presentation of the proposed sensor and an explanation of its sensing principle are provided in Section II. In Section III, a mathematical model of the resonant structure that includes nonlinear effects is developed in order to predict the sensor's sensitivity to an external force. Section IV reports the fabrication and characterization of a first prototype. Experiments conducted on lobster eggs are also included. Finally, Section V discusses future work and concludes the paper.

II. SENSOR DESCRIPTION

A. Concept

The proposed force sensor acts as a cell substrate sensitive to out-of-plane (normal) forces. As depicted in Fig.1, it consists of a monolithic structure clamped at its extremities.

D. Desmaële is with the CEA, LIST, Sensory and Ambient Interfaces Laboratory, 18 Route du Panorama, BP6, Fontenay-aux-Roses, F-92265, France denis.desmaele@cea.fr

M. Boukallel is with the CEA, LIST, Sensory and Ambient Interfaces Laboratory, 18 Route du Panorama, BP6, Fontenay-aux-Roses, F-92265, France mehdi.boukallel@cea.fr

Stéphane Régnier is with the Institut des Systèmes Intelligents et de Robotique, Université Pierre et Marie Curie, CNRS UMR 7222, 4 Place Jussieu, Paris, 75005, France stephane.regnier@upmc.fr

The structure also incorporates two rectangular apertures. Thereby, it can actually be viewed as two cantilevers serially linked via three parallel beams, the central beam being wider than the two outer beams.

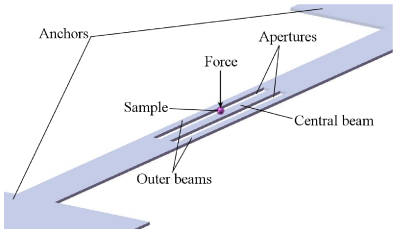

Fig. 1. Concept of the force sensitive surface illustrated with a suspended cell (trapping system for maintaining the cell not represented).

As compared to conventional strain-gauge based sensors, resonance phenomena allow for higher force sensitivities. Finite element analysis (FEA) conducted with COMSOL V.4 shows that if the structure of Fig.1 is mechanically excited at a proper frequency, it offers an antisymmetrical vibration mode where the two outer beams oscillate in antiphase. Meanwhile, the central beam remains immovable (see Fig.2).

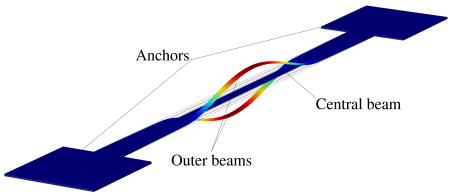

Fig. 2. Vibration mode exploited for the force sensitive surface: the outer beams oscillate in antiphase while the central beam remains immovable.

This balanced mode is of particular interest. Indeed, it enables high sensitivity rates offered by resonators without exposing cells to vibrations. Thereby, the area located at the half span of the central beam can be coated with biochemicals in order to culture and inject a few adherent cells. Alternatively, one might envision to use the central steady beam to implement a trapping system to grab and hold suspended cells.

B. Sensing principle

Conceptually, if a static force normal to the structure's plane is applied to the half span of the central beam, the whole structure deflects. Therefore, the outer beams are forced to deflect as well. When the outer beams oscillate as illustrated in Fig.2, interactions between static and dynamic behaviors occur. Thereby, the static deflection imposed by the normal force affects their initial resonance frequency. In fact, even slight static pre-deflection of beam resonators may significantly impact their dynamics [9]. Accordingly, it is possible to recover the magnitude of the normal force applied upon the central beam by monitoring frequency shifts of the outer beams.

III. ANALYTICAL MODEL

A. Nonlinear static deflections

To predict frequency shifts engendered by a normal force F applied to the central beam, static and dynamic behaviors are studied independently. The static analysis is first conducted in order to detail how the outer beams exactly behave during the deflection of the whole structure. Due to symmetry, our analysis can be limited to one fourth of the structure (see Fig.3).

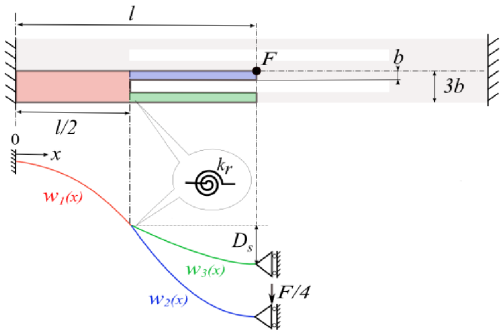

Fig. 3. Top: for predicting the quasi-static deflection of the structure, only the coloured *"tuning fork"* is considered. Bottom: equivalent one-dimensional model of the colored beams (proportions exaggerated for illustration purposes).

This quarter structure, similar in shape to a tuning fork, is composed of three segments: the overhang (colored in red), the central tine (colored in blue), and the outer tine (colored in green). All segments are assumed to satisfy Bernouilli's beam theory. To model the flexural displacement of each segment $w_{1,2,3}(x)$, second order polynomial expressions are chosen. At $x = 0$, the overhang is clamped so that the displacement $w_1(0)$ and the slope $\frac{d}{dx}w_1(0)$ are zero. Likewise, geometrical and mechanical constraints can be considered for each segment extremity. In so doing, eight of the nine unknown constants can be eliminated. Thereby, the three polynomials can be expressed with respect to a single free parameter a_2

$$\begin{cases} w_1(x) = a_2\, x^2 \\ w_2(x) = \dfrac{a_2}{2}\left(-2x^2 + 4lx - l^2\right) \\ w_3(x) = \dfrac{a_2}{4}\left[l^2 - \dfrac{6lk_r\left(4x^2 - 8lx + 3l^2\right)}{6lk_r + Ebh^3}\right] \end{cases} \tag{1}$$

where the length l and the width b are defined in Fig.3, E is the Young's modulus and h is the structure's thickness. Because F is solely applied upon the central tine, segments $w_2(x)$ and $w_3(x)$ should have different deflection amplitudes and deflection slopes. To consider this effect, the outer tine is supposed to be linked to the overhang at $x = l/2$ via a rotational spring whose stiffness is noted k_r.

With (1), we use an energy approach to derive the relationship governing the maximum displacement of the outer tine when the force F is applied at the extremity of the central

tine. During deflection, the potential energy stored by the tuning fork is

$$U_{tf} = U_b + U_s \tag{2}$$

where $U_b = U_{b_1} + U_{b_2} + U_{b_3}$ is the sum of strain energies developed by each segment during bending. For the overhang, we have

$$U_{b_1} = \frac{EI_1}{2} \int_0^{l/2} \left(\frac{d^2 w_1}{dx^2} \right)^2 dx \tag{3}$$

whereas the bending energy for each tine is

$$U_{b_i} = \frac{EI_i}{2} \int_{l/2}^{l} \left(\frac{d^2 w_i}{dx^2} \right)^2 dx \qquad i = 2,3 \tag{4}$$

In (3-4), $I_1 = bh^3/4$ and $I_2 = I_3 = bh^3/12$.

Similarly, $U_s = U_{s_1} + U_{s_2} + U_{s_3}$ is the sum of energy contributions due to axial stretching of the segments. For the overhang, this contribution is evaluated as follows

$$U_{s_1} = \frac{EA_1}{4\,l} \left[\int_0^{l/2} \left(\frac{dw_1}{dx} \right)^2 dx \right]^2 \tag{5}$$

whereas the potential energy due to the elongation of each tine is

$$U_{s_i} = \frac{EA_i}{4\,l} \left[\int_{l/2}^{l} \left(\frac{dw_i}{dx} \right)^2 dx \right]^2 \qquad i = 2,3 \tag{6}$$

In (5-6), $A_1 = 3bh$, and $A_2 = A_3 = bh$ represent the cross section areas of the three segments.

By considering the work $W = F w_2(l)$ done by the punctual force F, the unknown parameter a_2 can be simply found by minimizing the total potential energy function $\Phi = U_{tf} - W$

$$\frac{d\Phi}{da_2} = 0. \tag{7}$$

To solve (7), the following numerical values were used: $l = 12.5$ mm, $b = 0.25$ mm, $h = 0.1$ mm, $E = 212$ GPa and $k_r = 0.7 \times 10^{-3}$ Nm/rd.

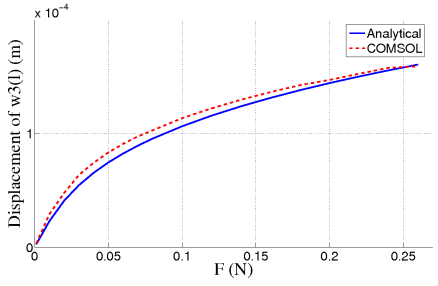

Fig. 4. Half span deflection of an outer beam for a normal force applied to the central beam.

To validate our modeling approach, FEA was used as a reference tool. COMSOL simulations were conducted in the nonlinear deflection mode with the values of l, b, h and E used to solve (7). In addition, we also specified a density of 8030 kg m^{-3} and a Poisson's ratio of 0.29 for the structure's material. Fig.4 compares FEA results with our theoretical approach. It is shown that the latter permits to predict with sufficient accuracy the half span deflection of an outer beam for a wide range of F. Fig.4 also clearly illustrates that the stretching (i.e., nonlinear) effect progressively dominates as the outer beam deflection increases above ~50% of the structure's thickness.

B. Dynamics of slightly curved outer beams

A dynamic analysis can now be carried out in order to predict how the static deflection imposed to the outer beams impacts their initial resonance frequency. Since we are only interested in the antisymmetrical vibration mode illustrated in Fig.2, we can actually grasp valuable insights on the structure's dynamics by restricting our study to a single outer beam (see Fig.5).

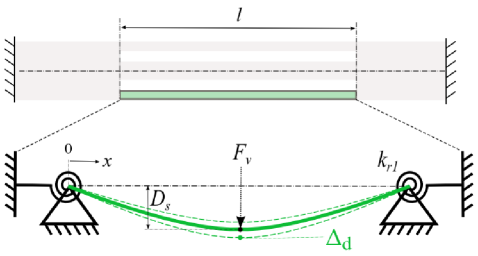

Fig. 5. For predicting frequency shifts, only one outer beam is considered. Vibrations (dashed green lines) take place around an equilibrium position (thick green line). The curved shape is indirectly engendered by static deflections (proportions exaggerated for illustration purposes).

Extremeties of the outer beam are connected to overhangs. Intuitively, we can foresee that the overhangs should slightly distort during oscillations of the outer beam. To a first approximation, we hence assume that the outer beam can be modeled as a hinged-hinged beam terminated by two rotational springs of stiffness k_{r_1}. For such boundary conditions, it is conventional to assume a displacement function in the form of a sine

$$w(x) = D_s \sin\left(\frac{\pi x}{l} \right) \tag{8}$$

where D_s is the half span deflection of the outer beam.

D_s is related to the force F applied upon the central steady beam, and can be estimated from the previous static analysis (see Fig.3)

$$D_s = w_3(l) - w_1(l/2). \tag{9}$$

Conceptually, it is however more convenient to consider that D_s is rather due to an unknown equivalent virtual force F_v directly applied at $w(l/2)$ (see Fig.5). With an energy approach, a relationship between D_s and F_v can be derived. Following a reasoning similar to the one detailed in (2-7) yields a *cubic force-centered-deflection law*

$$F_v = k_1\, D_s + k_3\, D_s^3 \tag{10}$$

where

$$k_1 = \frac{Ebh^3\pi^4}{24l^3} + \frac{2k_{r_1}\pi^2}{l^2} \quad \text{and} \quad k_3 = \frac{Ebh\pi^4}{8l^3}. \tag{11}$$

In (11), k_1 and k_3 are linear and nonlinear spring constants, respectively.

As in [10], we assume that small deflections of the beam about a mean deflection D_s can be described approximately by a single stiffness value. An effective spring constant is found by deflecting the beam from its equilibrium position by an arbitrary amount Δ_d (see Fig.5), so that

$$F_v = k_1 (D_s + \Delta_d) + k_3 (D_s + \Delta_d)^3. \tag{12}$$

Considering that vibration amplitudes Δ_d are sufficiently small, terms proportional to Δ_d^2 and Δ_d^3 in (12) may be neglected. Then, an equivalent stiffness of the outer beam may be approximated by

$$k_{eq} = \frac{dF_v}{d\Delta_d} \approx k_1 + 3\,k_3\,D_s^2. \tag{13}$$

As often in structures involving coupled beams, vibrating beams can be modeled to a first approximation as one degree of freedom oscillators (e.g., [11]). If we consider that our single outer beam oscillates as an undamped lumped-parameter system, the static deflection D_s affects its natural frequency as follows

$$\frac{f}{f_0} \approx \left[1 + \frac{3\,k_3}{k_1}\,D_s^2\right]^{1/2}. \tag{14}$$

In (14), D_s can be computed with (9) for different values of F applied upon the central beam. Frequency variations predicted by (14) are compared to FEA results in Fig.6. COMSOL simulations were run for the whole structure, as represented in Fig.2. Comparatively, (14) only considers one outer beam with approximate boundary conditions. Despite these simplifications, Fig.6 shows that with $k_{r1} = 10.5 \times 10^{-3}$ Nm/rd, (14) is accurate enough to predict the frequency shift engendered by F.

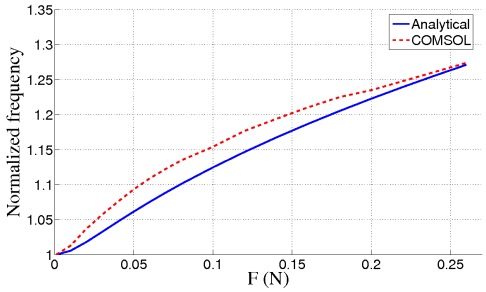

Fig. 6. Frequency shift of the outer beams predicted when a normal force F is imposed upon the central beam.

IV. EXPERIMENTS

A. Prototype fabrication

As a proof of concept, we fabricated a first experimental prototype intended to the study of cells whose diameter approximately ranges from 100 to 600 μm (see Fig.7). This monolithic prototype was fabricated from a single sheet of biocompatible stainless steel using wire cut electric discharge machining. All dimensions are those used for the analytical model. Mechanical excitation was provided by a 3 mm long, 2 mm wide and 200 μm thick piezoelectric (PZT) element (Physik Instrumente PIC151). The latter was bonded onto the structure with conductive paste and driven by an AC signal with a function generator (Agilent 33120A) connected to a laboratory power amplifier (NPA LPA400). During experiments, the prototype was suspended between two clamping jaws. One of them was fixed to a manual micropositioning stage that allowed horizontal translations.

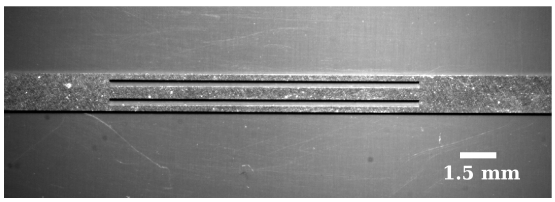

Fig. 7. Close-up of the experimental prototype manufactured (PZT element not visible).

B. Optical fiber vibrometer

To monitor the frequency of the two outer beams during experiments, we developed an extrinsic optical fiber displacement sensor similar to the ones reported in [12], [13]. We favoured this non-contact measurement technique in order to avoid any alteration of the mode shape of interest.

As illustrated in Fig.8, the implemented sensing head is made of two optical fibers. One of the fiber is used as a transmitter, namely it guides the light from a light source toward a reflective target. The second fiber is used as a receiver and collects the light reflected by the target. Step index multimode fibers with a cladding diameter of 125 μm and a numerical aperture of 0.22 were used (Thorlabs AFS50/125Y). However, cleaving of the fibers' extremities removed the cladding and reduced their diameter to 50 μm (core diameter). Such dimensions offered a compact sensing head with high capabilities of integration.

For the light source, we used a low-cost VSCEL diode (Honeywell HFE4080-321-XBA) originally intended for high-speed data communications. Since this diode emitted a light centered around 850 nm, ambient light could not disturb the signal of interest. Supplied with a forward current of 11 mA, this diode provided an optical power of 800 μW at the end of the transmitting fiber.

At the receiving side, the fiber was connected to a photodetector incorporating a photodiode and a transimpedance amplifier (Thorlabs PDA-10CF). This allowed to convert

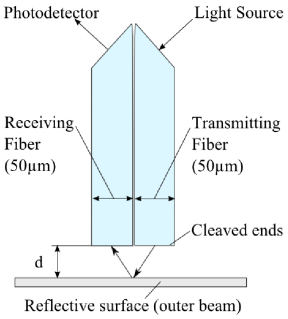

Fig. 8. Illustration of the double-fiber displacement sensor used to measure the oscillation amplitude of the outer beams during experiments.

light into a proportional electric signal. This photodetector offered a responsivity of 0.2 A/W at 850 nm.

To test and characterize our double-fiber sensor, we used our prototype (see Fig.7) as reflective target. To control the gap d between the sensing head and the prototype's surface, we used a micropositioning stage offering nanometric resolution (Physik Instrumente M112-1DG). Normalized variations of light intensity captured by the receiving fiber are plotted in Fig.9.

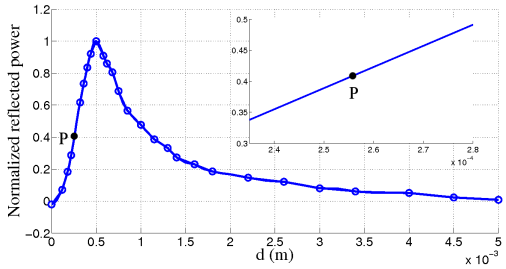

Fig. 9. Experimental variations of light intensity captured by the receiving fiber. The inset shows a magnified view of the linear area offered around P.

These light variations correspond exactly to theoretical predictions provided in [14]. This confirms that our double-fiber sensor was properly aligned and worked correctly.

C. Characterization of prototype's performances

For characterizing the prototype, we first sought to evaluate some of its intrinsic performances with no force applied to the central beam (unloaded conditions). To this end, we first positioned the double-fiber sensor 250 μm above the outer beams. This gap was set to exploit the steep linear slope offered around P in Fig.9. The amplified photodetector Thorlabs PDA-10CF was tuned to provide a gain of 70 dB. Thereby, the double-fiber sensor offered a linear sensitivity of 9 mV/μm.

The prototype was then vibrated with the PZT element. The antisymmetrical mode (see Fig.2) was found at 3180 Hz. When the PZT was driven with a peak-peak AC signal of 9 V, the maximum oscillation amplitude of the outer beams was 11 μm. Potential vibrations at the half span of the central beam were also checked. They never exceeded 400 nm, namely 2% of the outer beams oscillation amplitude.

In addition, we also explored the frequency response of the antisymmetrical mode. In ambient conditions (i.e., in air), a quality factor of $\sim$700 was obtained. Fig.10 confirms the linear vibrations of the structure since the curve is not distorted by hysteresis. Indeed, the small reported oscillation amplitude prevented the occurrence of nonlinearities such as spring softening or spring hardening effects [15].

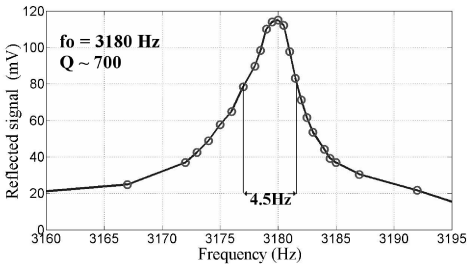

Fig. 10. Blown-up of the frequency response for the antisymetrical mode of vibrations (see Fig.2).

To load the structure, we actually could not apply a calibrated force during experiments. Instead, we bent the central beam with an indenter terminated by a metal bead whose diameter was 500 μm. The stiffness of the metal bead was much higher than the stiffness of the prototype. The indenter was translated by displacement steps of 10 μm via a second micropositioning stage (Physik Instrumente M112-1DG). Thanks to the high quality factor of the structure, each displacement increment imposed to the central beam caused drastic amplitude changes in the oscillation amplitude of the resonant outer beams. These easily detectable amplitude changes permitted to recover frequency shifts, as detailed in [16].

The full dynamic range of the prototype was discovered by bending the central beam up to 250 μm. The induced frequency shift is shown in Fig.11. The curve exhibits a linear sensitivity of $\sim$5.75 Hz/μm around S. Moreover, it is worth noting that results were repeatable even if the indenter was not perfectly positioned at the half span of the central beam.

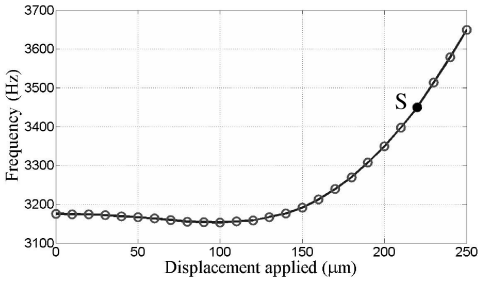

Fig. 11. Experimental frequency shift measured for a normal displacement applied to the half span of the central beam.

D. Biological applications

To demonstrate the possibility to use our force sensitive substrate in cell indentation or cell injection tasks, we applied a force on lobster eggs and measured the induced frequency

shift. Eggs were sorted to have an approximate diameter of 500 μm. To take advantage of the high sensitivity offered by our prototype, we needed to force it to stay in a static equilibrium around the point S (see Fig.11). To this end, we bent the central beam with the indenter. We then axially compressed the whole structure by translating the clamping jaw fixed to the manual positioning stage. Due to this slight axial compression, the resonance frequency dropped to 3080 Hz. However, this compression did not change the dynamic behavior of the prototype.

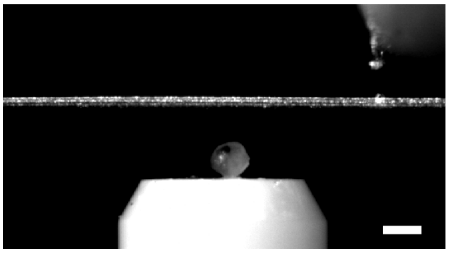

Fig. 12. Side view of the slightly curved prototype for measuring the force applied upon a lobster egg. The latter lies on an optical fiber connector ferrule. The double-fiber sensor is visible in the upper right corner. Scale bar represents 500 μm.

Since our current prototype does not include a system able to hold a suspended cell, lobster eggs were not directly placed on the central beam, as depicted in Fig.1. Instead, we preferred to replace the aforementioned indenter by an optical fiber connector ferrule (1.25 mm radius). We then cautiously placed the eggs on the ferrule (see Fig.12). The eggs were then gently pressed upon the central beam by translating the ferrule. The frequency shift measured during the squeezing of one egg is shown in Fig.13. Although the frequency shift reported varies with respect to a displacement, the amount of force applied upon the egg could be recovered via the structure's compliance.

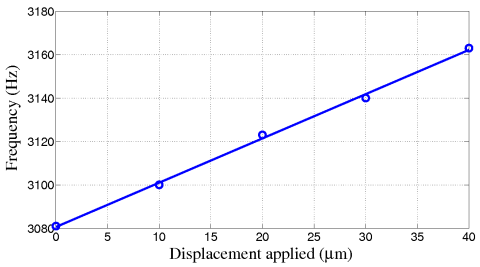

Fig. 13. Measured (o) and fitted (solid line) frequency shift for one lobster egg pressed against the central beam.

V. CONCLUSION AND FUTURE WORK

This paper has presented the design and fabrication of a novel type of force sensor intended to cell indentation and cell injection tasks. A first prototype has been characterized. Tests for measuring forces applied on lobster eggs have also been conducted. Performance characteristics reported are encouraging, even though limitations still have to be addressed. In particular, as for all types of resonators, our current prototype is very sensitive to boundary conditions. Thereby, it remains presently difficult to obtain repeatable results due to our current clamping system. Likewise, maintaining the structure in a slightly curved position turns out to be a delicate task. However, it is expected that these problems will be partly overcome via microfabrication processes. Indeed, miniaturization of the system will constitute the next step in order to target smaller cells. In the near future, we will also have to consider the fact that cells should ideally be maintained in cell medium providing vital nutrients during biomanipulation tasks. Because liquids can drastically impact resonators' performances, the consideration of such an environment will constitute the next key step in the development of our structure for its successful integration in a workable platform.

REFERENCES

[1] Y. Xie, D. Sun, C. Liu, and S. H. Cheng, "An adaptive impedance force control approach for robotic cell microinjection," in *IEEE/RSJ Int. Conf. on Intelligent Robots and Systems*, Nice, France, September 22-26, 2008, pp. 907–912.

[2] Y. Sun, B. J. Nelson, and M. Greminger, "Investigating protein structure change in the zona pellucida with a microrobotic system," *Int. J. Robot. Res.*, vol. 24, no. 2–3, pp. 211–218, 2005.

[3] D.-H. Kim, S. Yun, and B. Kim, "Mechanical force response of single living cells using microrobotic system," in *Int. Conf. on Robotics and Automation*, New Orleans, LA, April 2004, pp. 5013–5018.

[4] A. Pillarisetti, W. Anjum, J. P. Desai, G. Friedman, and A. D. Brooks, "Force feedback interface for cell injection," in *Joint Eurohaptics Conf. Symp. on Haptic Interfaces for Virtual Environment and Teleoperator Syst.*, Pisa, Italy, March 18-20, 2005, pp. 391–400.

[5] Y. Xie, D. Sun, and C. Liu, "Penetration force measurement and control in robotic cell microinjection," in *IEEE/RSJ Int. Conf. on Intelligent Robots and Syst.*, St. Louis, USA, October, 11-15, 2009, pp. 4701–4706.

[6] Y. Sun, K.-T. Wan, K. P. Roberts, J. C. Bischof, and B. J. Nelson, "Mechanical property characterization of mouse zona pellucida," *IEEE Trans. Nanobiosci.*, vol. 2, no. 4, pp. 279–286, 2003.

[7] X. Liu, Y. Sun, W. Wang, and B. Lansdorp, "Vision-based cellular force measurement using an elastic microfabricated device," *J. Micromech. Microeng.*, vol. 17, no. 7, pp. 1281–1288, 2007.

[8] A. Meister, M. Gabi, P. Behr, P. Studer, J. Vörös, P. Niedermann, J. Bitterli, J. Polesel-Maris, M. Liley, H. Heinzelmann, and T. Zambelli, "FluidFM: combining atomic force microscopy and nanofluidics in a universal delivery system for single cell applications and beyond," *Nano Lett.*, vol. 9, no. 6, pp. 2501–2507, 2009.

[9] F. Treyssède, "Prebending effects upon the vibrational modes of thermally prestressed planar beams," *J. Sound Vib.*, vol. 307, pp. 295–311, 2007.

[10] D. J. Morris, J. M. Yougsman, M. J. Anderson, and D. F. Bahr, "A resonant frequency tunable, extensional mode piezoeletric vibration harvesting mechanism," *Smart Mater. Struct.*, vol. 17, p. 065021 (8pp), 2008.

[11] N. Lobontiu, *Dynamics of Microelectromechanical Systems*, ser. Microsystems. Springer, 2007, vol. 17, ch. 4, pp. 351–356.

[12] S. Binu, V. P. Mahadevan Pillai, and N. Chandrasekaran, "Fibre optic displacement sensor for the measurement of amplitude and frequency vibration," *Opt. Laser Technol.*, vol. 39, pp. 1537–1543, 2007.

[13] G. Perrone and A. Vallan, "A low-cost optical sensor for noncontact vibration measurements," *IEEE Trans. Instrum. Meas.*, vol. 58, pp. 1650–1656, May 2009.

[14] J. B. Faria, "A theoretical analysis of the bifurcated fiber bundle displacement sensor," *IEEE Trans. Instrum. Meas.*, vol. 47, no. 3, pp. 742–747, June 1998.

[15] L. C. Shao, M. Palaniapan, and W. W. Tan, "The nonlinearity cancellation phenomenon in micromechanical resonators," *J. Micromech. Microeng.*, vol. 18, p. 065014 (9pp), 2008.

[16] K. Fukuzawa, T. Ando, M. Shibamoto, Y. Mitsuya, and H. Zhang, "Monolithically fabricated double-ended tuning fork based force sensor," *J. Appl. Phys.*, vol. 99, p. 094901 (5pp), 2006.